Quantification of the disorder in network-modified silicate glasses

I. Farnan*, P. J. Grandinetti†, J. H. Baltisberger†, J. F. Stebbins*, U. Werner†, M. A. Eastman† & A. Pines†

* Department of Geology, Stanford University, Stanford, California 94305, USA
† Materials Science Division, Lawrence Berkeley Laboratory, 1 Cyclotron Road, Berkeley, California 94720, USA and Department of Chemistry, University of California, Berkeley, California 94720, USA

Local order in silicate glasses has been observed by many experimental techniques to be similar to that in crystalline materials. Details of the intermediate-range order are more elusive, but essential for understanding the lack of long-range symmetry in glasses and the effect of composition on glass structure. Two-dimensional ^{17}O dynamic-angle-spinning nuclear magnetic resonance experiments reveal intermediate-range order in the distribution of inter-tetrahedral (Si–O–Si) bond angles and a high degree of order in the disposition of oxygen atoms around the network-modifying cations.

THE difference between a glass and a crystal lies in disorder present in the intermediate-range glass structure that eliminates long-range translational symmetry. Characterization of this disorder is an important experimental objective because it is a critical test of the accuracy of models of glass structure. In network-modified silicate glasses, the continuous disordered network of SiO_4 tetrahedra is presumed to be disrupted by modifying cations which create nonbridging oxygens (oxygens bonded to one silicon atom). Two principal sources of disorder are thought to be this disruption of the network and the range of bond angles (Si–O–Si) between network-forming cations. It is well established experimentally that silicon and oxygen are ordered locally in silicate glasses, and that SiO_4 tetrahedra are the basic structural units just as they are in low-pressure crystalline silicates. From extended X-ray absorption fine structure (EXAFS) studies of modifier cations, we know that they too are regularly coordinated by oxygen[1,2], having coordination polyhedra and bond lengths similar to those in crystalline silicates. Isotopically substituted neutron scattering has also shown that ordering associated with modifier cations extends beyond the first coordination sphere, by detecting strong correlations between Ca–Ca as well as Ca–O distances in $CaSiO_3$ glass[3,4]. This is consistent with ^{29}Si nuclear magnetic resonance (NMR) studies of silicate glasses, which show that the distribution of nonbridging oxygens is not random, being close to binary[5]; the deviation from a binary distribution depends on the electronegativity of the network modifier and on the glass transition temperature[6]. Taken together, these experimental data indicate considerable order associated with network modification. Quantification of the remaining disorder associated with variations in bridging angles between network-forming cations is therefore important. For unmodified SiO_2 glass, the X-ray scattering radial distribution function[7] and correlations between ^{29}Si NMR chemical shifts and average Si–O–Si bond angles[8,9] have been used to derive the inter-tetrahedral (Si–O–Si) bond-angle distribution. Both of these methods encounter problems when extended to compositionally more-complex modified glasses. Almost all technologically or geochemically important glass compositions are more complex than SiO_2. The ability to describe and quantify the microscopic structure of these materials (beyond the first coordination sphere) as a function of composition will considerably advance the understanding of their structure and properties.

Volumetrically, silicate glasses are dominated by oxygen anions, yet despite this the structure of silicate glasses has been studied almost entirely from the perspective of the cations and their coordination. For example, X-ray scattering experiments are most sensitive to scattering from cations (network-forming and network-modifying) that are heavier than oxygen anions, EXAFS experiments concentrate on network modifiers such as Na^+ or Ca^{2+}, and ^{29}Si NMR experiments specifically observe the signal from the network-forming cation. Here we investigate the local environments of these oxygen anions. As oxygen is the connecting atom between locally ordered SiO_4 tetrahedra, and between silicon and network-modifying cations which are also thought to have locally ordered environments, the intermediate-range disorder in the glass will be reflected in the range of environments exhibited by these oxygen atoms. Oxygen-17 NMR is a sensitive and direct way to characterize these interconnections. Spectral resolution in previous ^{17}O NMR studies of silicate glasses[10,11] was seriously reduced by anisotropic interactions between ^{17}O nuclei and electric field gradients (EFGs) at oxygen sites. Line broadenings caused by a distribution of oxygen environments contained information on the disorder in the glass but were convolved with the anisotropic quadrupolar broadening, which could not be removed by the magic-angle-spinning technique[12]. In contrast, two-dimensional dynamic angle spinning (DAS)[13] can produce high-resolution ^{17}O NMR spectra of crystalline silicates. Similar experiments on silicate glasses should provide isotropic ^{17}O chemical and quadrupolar shifts that have the potential to identify bridging and nonbridging oxygens, discriminate between oxygens bonded to different network modifiers and provide details of the ordering of those modifiers around the nonbridging oxygens. Additional insight into the structure of these glasses is available in the anisotropic second dimension of the two-dimensional (2-D) NMR spectrum, where anisotropic line shapes can be correlated with oxygen site symmetries.

We present ^{17}O NMR results for potassium and potassium–magnesium silicate glasses that indicate a high degree of ordering of network-modifying cations around nonbridging oxygens even when two network modifiers are present. Although ordering of single network-modifying cations in silicate glasses may be expected from previous neutron-scattering experiments[3,4], substantially more order is implied here as two different cations order about the nonbridging oxygens. In both glasses there is a high degree of uniformity in nonbridging oxygen environments, with oxygens that bridge SiO_4 tetrahedra having a greater range of environments than those that bond to network modifiers. Presumably, without the constraint of long-range symmetry the structure can relax locally around the modifier, with most of the disorder being assumed by the distribution in intertetrahedral Si–O–Si angles. This bond-angle distribution can be determined by combining the information on the oxygen

site symmetry available from the 2-D NMR experiment with correlations between the asymmetry and magnitude of the EFG at the bridging oxygen and the Si–O–Si bond angle. Such detailed structural information should provide accurate data for modelling and allow experimental evaluation of the effect of pressure and temperature (glass transition temperature) on vitreous SiO_2 and modified silicate glasses of complex composition. In addition, this method probes the network-forming anion and so should be applicable to any oxide glasses.

Experimental methods

NMR frequency shifts introduced by magnetic or electric interactions due to local atomic structure are generally anisotropic: the shift depends on the orientation of the atomic site with respect to the external magnetic field. In powdered or amorphous solids, all possible orientations of sites are present, and the superposition of resonances from all orientations produces broad anisotropic line shapes. To achieve high-resolution NMR in this situation, the broadening can be removed by rapid sample spinning at specific angles to the magnetic field. The relative orientation of the site and the magnetic field become time-dependent, and the broadening interaction is averaged away either completely or to a single scalar (isotropic) value. For broadening interactions small enough (compared with the interaction with the external magnetic field) to be described to first order, such as chemical shift anisotropy, spinning the sample about a single axis inclined at an angle of 54.7° to the magnetic field (magic angle spinning) will result in a high-resolution spectrum. In general, however, the interaction between the quadrupole moment of ^{17}O and the EFGs at oxygen sites is large enough that second-order broadenings are substantial and they can only be completely removed by spinning the sample about two axes[12], as in the recently developed DAS NMR technique[13–15]. DAS is intrinsically a two-dimensional experiment and provides a correlation between high-resolution isotropic spectra in the ω_1 dimension, where all anisotropic broadening is removed (each oxygen site has a characteristic isotropic chemical and second-order quadrupolar shift), and anisotropic site symmetry information in the ω_2 line shape.

We prepared two silicate glasses of composition $K_2Si_4O_9$ and $KMg_{0.5}Si_4O_9$ with nominal ^{17}O enrichments of 35 and 41%, respectively. These compositions were chosen to test the ability of the DAS NMR technique to distinguish oxygens bonded to different network-modifying cations as well as between bridging and nonbridging oxygens. Oxygen-17 DAS spectra were acquired for both samples using a home-built probe[16] in commercial wide-bore magnets with fields of 9.4 and 11.7 T. The 2-D ^{17}O NMR spectrum of $K_2Si_4O_9$ glass is shown in Fig. 1*a*. Resonances characteristic of bridging (6 p.p.m.) and nonbridging (64 p.p.m.) oxygens in the glass are clearly resolved in the isotropic spectrum (projection of the 2-D spectrum onto the ω_1 axis) and the 2-D plot. The 2-D plot also shows structure in the bridging oxygen resonance in the anisotropic dimension (ω_2) with the line shape spreading out towards higher frequency in ω_1. The isotropic linewidths, which are roughly an order of magnitude greater than those obtained for ^{17}O DAS NMR in crystalline silicates, are due solely to distributions in the environments of the bridging and nonbridging oxygens and so directly reflect the disorder associated with each oxygen type.

Ordering of network modifiers

The range of environments displayed by a nonbridging oxygen will reflect both the distribution of network modifiers throughout the sample and the regularity of the individual network-modifier environments. The isotropic ^{17}O DAS NMR resonance of the nonbridging oxygen in $K_2Si_4O_9$ glass (Fig. 1*a*) at 64 p.p.m. is 17 p.p.m. wide (full width at half maximum, FWHM). A distribution of isotropic quadrupolar and chemical shifts for each oxygen site is responsible for this width. In previous studies of crystals, the chemical and quadrupolar shifts of unique sites were separated by taking advantage of the inverse magnetic field dependence of the second-order quadrupolar interaction[17] and doing the experiment at two magnetic fields. The chemical shift may then be determined by extrapolation to infinite magnetic field where the quadrupolar shift becomes zero. The exact chemical shift distribution in a glass cannot be derived by extrapolation, or mapping, to infinite magnetic field in this way without prior knowledge of the relationship between the chemical shift and quadrupole parameters for the oxygen sites. The change in FWHM with magnetic field should however allow us to obtain a FWHM for the distribution of chemical shifts. The nonbridging line in $K_2Si_4O_9$ glass at 11.7 T (not shown) is 15 p.p.m. wide, and this, combined with the 9.4-T data, indicates a range of chemical shifts of 13 p.p.m. This range is narrow compared with that of nonbridging oxygens in crystalline silicates[18] where ^{17}O chemical shifts of oxygens bonded to single

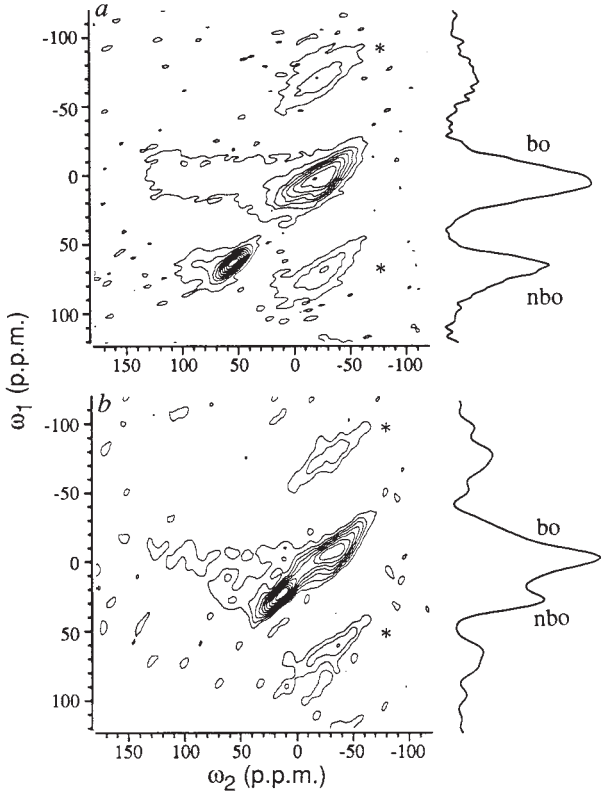

FIG. 1 Two-dimensional ^{17}O DAS NMR spectra and projections onto the isotropic axis (ω_1) of modified silicate glasses at 9.4 T (54.245 MHz): *a*, $K_2Si_4O_9$, *b*, $KMg_{0.5}Si_4O_9$. The resonances of bridging oxygens (bo), nonbridging oxygens (nbo) and sidebands (*) that arise from spinning slower than the width of the static anisotropic line are marked. The spectrum is obtained by spinning the sample sequentially about two axes inclined at angles θ_1 (37.38°) and θ_2 (79.19°) to the external magnetic field. The angles are chosen so that the anisotropic evolution of the ^{17}O spin magnetization at θ_1 is the inverse of that at θ_2 and is thus completely cancelled during evolution at the second angle. By incrementing the evolution time t_1 at angle θ_1 and detecting each NMR signal $S(t_2)$ while spinning about angle θ_2, we obtain a 2-D interferogram $S(t_1, t_2)$ which can be Fourier-transformed and phase-corrected to produce a 2-D frequency spectrum containing an isotropic dimension (ω_1) and an anisotropic dimension (ω_2). This produces anisotropic line shapes in ω_2 characteristic of spinning about an angle of 79.19° to the magnetic field. These are due almost entirely to the interaction between the quadrupole moment of ^{17}O and the EFG at the oxygen sites, and have shapes that depend on the symmetry (characterized by the asymmetry parameter, η) and widths that depend on the magnitude of the EFG. Selective pulses that excited the ^{17}O central transition and delays of 4 s were used to collect ~$50t_1$ points. The t_1 dimension was zero-filled to 256 points and a 200-Hz gaussian line broadening was applied in the t_2 dimension before Fourier transformation of a 256×256 data matrix.

modifier cations can range up to 27 p.p.m. in wollastonite ($CaSiO_3$) and 23 p.p.m. in forsterite (Mg_2SiO_4). It does seem that there is a greater range of (discrete) nonbridging oxygen environments in crystalline silicates than in the glasses studied here, although the variation in ^{17}O chemical shift with field strength of the modifier cation may not be the same. The implication is that the lack of long-range symmetry constraints in a glass allows local structural relaxation around network modifiers and produces more-uniform nonbridging oxygen environments.

The disorder associated with nonbridging oxygens might be expected to increase if we were to introduce an additional modifier into the tetrasilicate composition glass. Figure 1*b* shows the spectrum of $KMg_{0.5}Si_4O_9$ glass at 9.4 T. The NMR line for the nonbridging oxygen shifts by 40 p.p.m. to lower frequency while retaining essentially the same width as the nonbridging oxygen peak in $K_2Si_4O_9$. Only one peak is observed, so there are no separate nonbridging oxygen environments due to K and Mg modifiers, nor any clustering of K and Mg. The similar width of the nonbridging oxygen peak in both glasses implies a high degree of ordering of K and Mg. Each nonbridging oxygen in the $KMg_{0.5}Si_4O_9$ glass must have a similar bonding environment, with the linewidth caused by similar variations in bond length and angle as in the single modifier glass. A random distribution of K and Mg, on the other hand, might be expected to produce a broad peak ranging from 64.0 to 25.0 p.p.m. (comparing the shifts of K and Mg nonbridging oxygens in crystalline materials[19,20]). In crystalline $K_2Si_4O_9$ (ref. 21) each nonbridging oxygen is in fivefold coordination with one silicon and four potassium neighbours. If the nonbridging oxygens in the glass have similar environments to the crystal an ordered substitution of one Mg^{2+} for two K^+ about each nonbridging oxygen is implied. For a K/Mg ratio of 2, the only way to produce an ordered arrangement of K^+ and Mg^{2+} in the glass is to have an original coordination of four K^+ about each nonbridging oxygen in $K_2Si_4O_9$. This fivefold coordination of the nonbridging oxygens in alkali silicate glasses is also predicted by recent molecular dynamics simulations[22]. The ordered substitution of Mg^{2+} in the tetrasilicate glass will reduce the nonbridging oxygen coordination number from five to four. We determine a change in the average chemical shift of 26 p.p.m. for the nonbridging oxygen site, from data at 11.7 T. This change is similar to that observed for changes in chemical shift with oxygen coordination number of cations such as Si or Al, but in the opposite direction: lower coordination is more shielded.

The uniform and ordered nonbridging oxygen environments observed here, together with experiments on the network modifiers themselves[1,3,4] that show 'unexpected' local order around these cations, indicate that the configuration 'frozen in' as a silicate liquid goes through the glass transition is one that corresponds to a minimum energy and high order for the network modifiers and nonbridging oxygens.

Inter-tetrahedral bond angles

In Fig. 1*a* and *b*, the 2-D spectrum of the bridging oxygen shows structure in the anisotropic dimension, with a systematic change in the anisotropic line shape across the isotropic line from low to high frequency. Slices parallel to the ω_2 axis (Fig. 2) show this change in line shape to be due to an increase in the asymmetry parameter (η) with increasing frequency in ω_1. The parameter η describes the symmetry of the EFG at the oxygen site. A physical interpretation of this behaviour is that low values of η (0 represents cylindrical symmetry) correspond to Si-O-Si bond angles close to 180°, and as the bond angle decreases the deviation from cylindrical symmetry increases, thus increasing η.

In contrast to η, the isotropic quadrupolar shift (to low frequency from the chemical shift) is almost entirely determined by the magnitude of the EFG (its asymmetry has a very small effect). Oxygens shifted to lower frequency in ω_1 have smaller values of η and those shifted to higher frequncy in ω_1 have larger values of η. This means that the oxygen EFG is a maximum for Si-O-Si bond angles of 180°, and decreases with bond angle. This interpretation is supported by *ab initio* molecular orbital calculations[23] of the variation of the oxygen EFG and η with the Si-O-Si bond angle (α) in the molecule $H_3Si\text{-}O\text{-}SiH_3$. Analysis of these calculated values shows a simple relationship: $\eta = 1 + \cos\alpha$. These calculated values of η are plotted along with this function in Fig. 3*a*. Two experimental values of η determined from careful fitting of bridging oxygen ^{17}O MAS NMR spectra of cristobalite (SiO_2) and wadeite $K_2Si_4O_9$ (a high-pressure polymorph of $K_2Si_4O_9$) also fall close to this line.

The observed line shapes in ω_2 may be analysed using a multi-parameter least-squares fitting procedure to extract η, the EFG and chemical shift for each slice (Fig. 2). The result of fitting the slice through the maximum of the bridging oxygen peak gives a value for the most probable angle in the Si-O-Si bond-angle distribution, $V(\alpha)$. For $K_2Si_4O_9$ glass this value is $\eta = 0.20$, which corresponds to a bond angle of 143°. To derive the entire bond-angle distribution we must transform the distribution in asymmetry parameters, $X(\eta)$, obtained from the 2-D NMR experiment to a distribution of bond angles, $V(\alpha)$, using the following equation[9]

$$V(\alpha) = X(\eta)|(d\eta/d\alpha)| \quad (1)$$

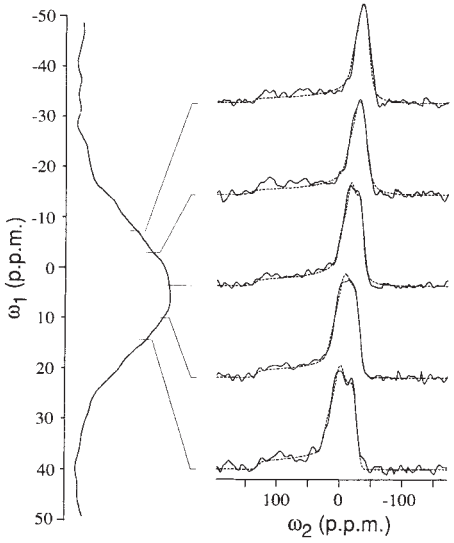

FIG. 2 Details of the bridging oxygen ^{17}O NMR resonance in $K_2Si_4O_9$ glass. Slices parallel to the ω_2 anisotropic axis (solid lines) are shown together with the results of multi-parameter least-squares fits (dotted lines) to obtain the variation of the magnitude and asymmetry of the electric field gradient across the isotropic line shape (ω_1). The residual chemical shift anisotropy and dipolar coupling present in the ω_2 line shape were approximated by a line-broadening parameter.

A partial Si-O-Si bond angle distribution, $V(\alpha)$, determined solely from our fitted values of η and the correlation of η with bond angle is shown by the black dots in Fig. 4. But the magnitude of the oxygen EFG also varies systematically with bond angle, according to theoretical calculations[23] and our own data. The magnitude of the oxygen EFG closely follows an empirical expression for the variation in oxygen *sp* hybridization with Si-O-Si angle[24], $(\cos\alpha/(\cos\alpha-1))$. Values of the EFG obtained from fits of ω_2 line shapes are plotted against the angle derived from the value of η obtained from the same fit in Fig. 3*b*. Also shown are the results of earlier molecular orbital calculations of oxygen EFG[23], where the absolute magnitude has been scaled to coincide with the experimental curve. This relationship between oxygen EFG and α may also be used to determine $V(\alpha)$ simply from the line shape in ω_1. The isotropic quadrupolar shift, $\delta_{iso}(Q)$ in equation (2) (where ν_L is the Larmor frequency and I the spin quantum number), obtained in ω_1 by subtracting the chemical shift from the total shift

$$\delta_{iso}(Q) = -\tfrac{3}{40}[(I(I+1)-\tfrac{3}{4})/I^2(2I-1)^2](P_q^2/\nu_L^2)\times 10^6 \quad (2)$$

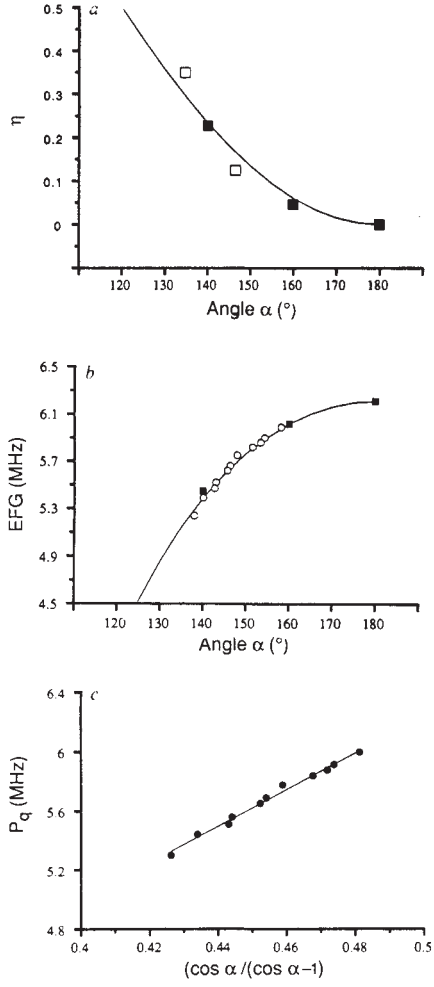

FIG. 3 Electric field gradient (EFG) parameters for bridging oxygens as a function of the Si-O-Si bond angle (α). *a*, Asymmetry parameter η. (■) calculated by Tossell and Lazzeretti[23], (□) experimental points for bridging oxygens in cristobalite ($\alpha=146.4°$)[33] and wadeite[15] ($\alpha=134.7°$). The solid line is the function $\eta=1+\cos\alpha$. *b*, Magnitude of EFG (○) for the fitted slices parallel to ω_2 in the $K_2Si_4O_9$ glass spectrum with the angle given by the fitted value of η. ■, The trend in calculated values from ref. 23 scaled to lie on the experimentally determined line. The solid line is the relationship $EFG(\alpha)=EFG(180°)\times 2(\cos\alpha/(\cos\alpha-1))$. *c*, Quadrupolar product P_q [$EFG\times(1+\frac{1}{3}\eta^2)^{1/2}$] determined from fits of ω_2 line shapes against $(\cos\alpha/(\cos\alpha-1))$. The straight line has a correlation coefficient of $r=0.995$.

depends on the quadrupolar product (P_q) of the magnitude of th oxygen EFG and its asymmetry, η

$$P_q = EFG\times(1+\tfrac{1}{3}\eta^2)^{1/2} \quad (3)$$

Because $(1+\frac{1}{3}\eta^2)^{1/2}$ is close to 1 ($0\leq\eta\leq 1$), P_q shows a similar correlation with $(\cos\alpha/(\cos\alpha-1))$ as the EFG (Fig. 3*c*). Consequently, $V(\alpha)$ can be obtained by two transformations, using equations similar to equation (1), from a distribution in $\delta_{iso}(Q)$ to a distribution in P_q and then to a distribution in α. This is the full distribution shown in Fig. 4.

The experimentally derived distribution $V(\alpha)$ for $K_2Si_4O_9$ glass has a peak at 143° and half-width of 21° from 135° to 156°. Mozzi and Warren[7] have derived an inter-tetrahedral bond-angle distribution for SiO_2 glass which is shown for comparison in Fig. 5. The $K_2Si_4O_9$ glass distribution is narrower but follows the shape of the Mozzi and Warren distribution with the peaks coinciding (144 and 143°) and both being skewed towards low angles and tailing off towards high angles. Both distributions probably reflect repulsion between Si atoms at low bond angles and a shallow dependence of energy on angle out to 180° (ref. 25).

The main difference between SiO_2 and $K_2Si_4O_9$ is the presence of nonbridging oxygens. Apart from the static structural effect introduced by the network modifier, the nonbridging oxygens created also provide a flow mechanism for the silicate liquid[26] which allows structural relaxation to occur more readily. In $K_2Si_4O_9$ glass, it seems that more Si-O-Si bonds are able to take up the energetically most favourable angle causing a narrowing of the total distribution. The flow mechanism involves a change in oxygen speciation from nonbridging to bridging (or vice versa) by means of the approach of a nonbridging oxygen to a silicate tetrahedron and the formation of a silicon intermediate with fivefold coordination[27]. It seems that when a nonbridging oxygen finds itself in an ordered arrangement with network modifiers, such as that observed by ^{17}O NMR in the glass, it becomes trapped in this low-energy configuration. It is then unavailable to take part in the structural relaxation mechanism. Presumably, as this happens throughout the liquid, structural relaxation is progressively inhibited and the glass transition occurs. The effect of the strength of the modifier oxygen bonds and the glass transition temperature on silicate glass structure

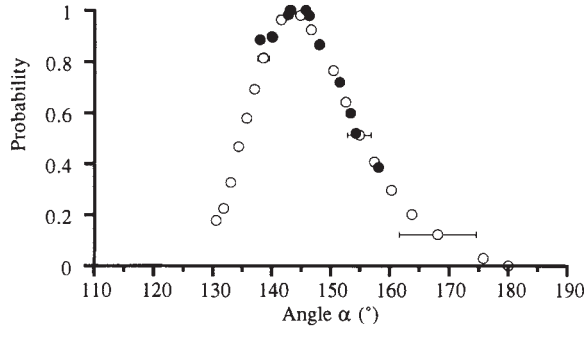

FIG. 4 Si-O-Si bond-angle distributions ($V(\alpha)$) for $K_2Si_4O_9$ glass (●) determined from fitted values of η. Less-probable bond angles have lower signal intensity and are difficult to fit, so only a partial bond-angle distribution is shown. (○) Determined from the relationship between P_q and Si-O-Si bond angle. P_q is determined from the isotropic quadrupolar shift in ω_1 ($\delta_{iso}(Q)$, equation (2)). Values of $\delta_{iso}(Q)$ beyond those obtained by fitting slices in ω_2 were separated from the chemical shift by extrapolation of a linear relationship between total shift and chemical shift for the fitted slices. Error bars on the distribution determined from P_q are propagated from the error in determining the isotropic quadrupolar shift and hence P_q. This results in greater uncertainty in the high bond angles because P_q is slowly varying as it approaches 180°.

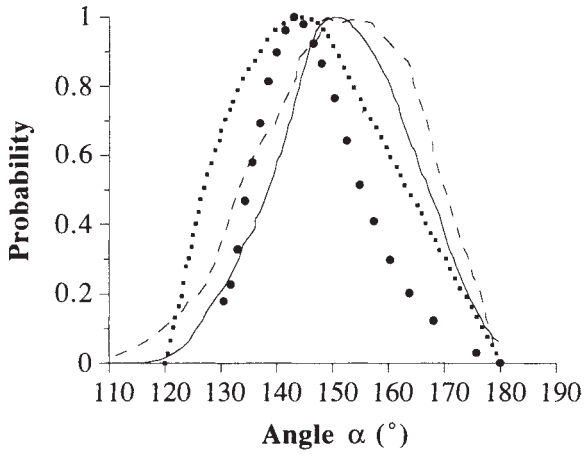

FIG. 5 Comparison of bond-angle distributions ($V(\alpha)$) for silicate glasses: ●, $K_2Si_4O_9$ reported here; ■, SiO_2 determined from the X-ray radial distribution function by Mozzi and Warren[7]. (----) $78K_2O{\cdot}216SiO_2$ produced by a molecular dynamics simulation with a two-body potential[29]; (——) $Na_2O{\cdot}2SiO_2$ produced by a molecular dynamics simulation using a three-body potential[31].

observed by means of the Si–O–Si bond-angle distribution should allow detailed investigation of these processes.

The bond-angle distribution for $K_2Si_4O_9$ glass does not show the bimodal bond-angle distribution with an additional peak at ~110° that was present in earlier molecular dynamics simulations of modified silicate glasses[28]. More-recent simulations of potassium silicate glasses[29,30] produce a bond-angle distribution that is opposite in overall shape (skewed to high angles) and much broader than the distribution here (Fig. 5). The broadness is certainly a result of the high quench rates (10^{14} K s^{-1}) and therefore high glass transition temperature of these simulated glasses. The opposite skewing probably reflects the nondirectional nature of the two-body potentials used. They cannot reproduce the repulsive effects that cause the rapid fall-off of the distribution to zero around 120°. Molecular dynamics simulations of sodium silicate glasses[31] employing three-body potentials are in better agreement but are still skewed towards high angle. Realistic quench rates, and therefore distribution widths, are unlikely in these simulations because of computer limitations, but overall reproduction of the shape of the distribution should be a good test of the potentials being used.

Prospects for future work

The ability to characterize the inter-tetrahedral bond-angle distribution should provide insight into the variation of glass structure with pressure and glass transition temperature and test the accuracy of model distributions derived from other experimental techniques and computer simulations. Because the technique probes the bridging angle locally, complex compositons do not cause problems as they do in scattering experiments where there are many overlapping pair correlation functions in the radial distirbution analysis. Silicon-29 NMR has also been used to derive Si–O–Si bond-angle distributions for SiO_2 glass[9,10,32] but it measures the average of four such angles at each SiO_4 tetrahedron and uses a correlation that does not hold if a tetrahedron contains a nonbridging oxygen. The distribution derived here is sensitive to each Si–O–Si bond and is not affected by nonbridging oxygens unless by coincidence they overlap the bridging oxygen resonance.

In general, similar 2-D NMR techniques could be applied to any material in which there are distributions of environments causing a broad NMR line in one dimension. By resolving the data into isotropic and anisotropic dimensions, we should find the additional symmetry and population information about site distribution very useful in characterizing sites in catalysts, amorphous semiconductors and incommensurate materials as well as glasses. □

Received 2 March; accepted 2 June 1992.

1. Greaves, G. N., Fontaine, A., Lagarde, P., Raoux, D. & Gurman, S. J. *Nature* **293,** 611–616 (1981).
2. Greaves, G. N. in *Glass Science and Technology* (eds Uhlman, D. R. & Kreidl, N. J.) Vol. 4B, 1–76 (1990).
3. Eckersley, M. C., Gaskell, P. H., Barnes, A. C. & Chieux, P. *Nature* **335,** 525–527 (1988).
4. Gaskell, P. H., Eckersley, M. C., Barnes, A. C. & Chieux, P. *Nature* **350,** 675–677 (1991).
5. Dupree, R., Holland, D., McMillan, P. W. & Pettifer, R. F. *J. non-cryst. Solids* **68,** 399–410 (1984).
6. Stebbins, J. F. *J. non-cryst. Solids* **106,** 359–369 (1988).
7. Mozzi, R. L. & Warren, B. E. *J. appl. Cryst.* **2,** 164–172 (1969).
8. Dupree, R. & Pettifer, R. F. *Nature* **308,** 523–525 (1984).
9. Pettifer, R. F., Dupree, R., Farnan, I. & Sternberg, U. *J. non-cryst. Solids* **106,** 408–412 (1988).
10. Geissberger, A. E. & Bray, P. J. *J. non-cryst. Solids* **54,** 121–137 (1983).
11. Kirkpatrick, R. J. *et al.* in *Structure and Bonding in Non-Crystalline Solids* (eds Walrafen, G. E. & Revesz, A. G.) (Plenum, New York, 1986).
12. Samoson, A., Lipmaa, E. & Pines, A. *Molec. Phys.* **65,** 1013–1018 (1988).
13. Chmelka, B. F. *et al. Nature* **339,** 42–43 (1989).
14. Lior, A. & Virlet, *J. Chem. Phys. Lett.* **152,** 248–253 (1988).
15. Mueller, K. T. *et al. J. magn. Reson.* **86,** 470–487 (1990).
16. Eastman, M. A., Grandinetti, P. J., Lee, Y. K. & Pines, A. *J. magn. Reson.* (in the press).
17. Cohen, M. H. & Reif, F. *Solid State Phys.* **5,** 321–438 (1957).
18. Mueller, K. T., Baltisberger, J. H., Wooten, E. W. & Pines, A. *J. phys. Chem.* (in the press).
19. Mueller, K. T., Wu, Y., Chmelka, B. F., Stebbins, J. F. & Pines, A. *J. Am. chem. Soc.* **113,** 32–38 (1991).
20. Xue, X., Stebbins, J. F. & Kanzaki, M. *Trans. Am. Geophys. Un.* **72,** 572 (1991).
21. Schweinsberg, H. & Liebau, F. *Acta cryst.* B**30,** 2206–2213 (1974).
22. Vessal, B. *et al. Nature* **356,** 504–506 (1992).
23. Tossell, J. A. & Lazzeretti, P. *Phys. Chem. Miner.* **15,** 564–569 (1988).
24. Engelhardt, G. & Radeglia, R. *Chem. Phys. Lett.* **108,** 271–274 (1984).
25. Newton, M. D. & Gibbs, G. V. *Phys. Chem. Miner.* **6,** 221–246 (1980).
26. Faman, I. & Stebbins, J. F. *J. Am. chem. Soc.* **112,** 32–39 (1990).
27. Stebbins, J. F. *Nature* **351,** 638–639 (1991).
28. Soules, T. E. *J. chem. Phys.* **71,** 4570–4578 (1979).
29. Huang, C. & Cormack, A. N. *J. chem. Phys.* **95,** 3634–3642 (1991).
30. Tesar, A. A. & Varshneya, A. K. *J. chem. Phys.* **87,** 2986–2989 (1987).
31. Melman, H. & Garofalini, S. H. *J. non-cryst. Solids* **134,** 107–115 (1991).
32. Gladden, L. F., Carpenter, T. A. & Elliott, S. R. *Phil. Mag.* B**53,** L81–L87 (1986).
33. Spearing, D. R., Farnan, I. & Stebbins, J. F. *Phys. Chem. Miner.* (in the press).

ACKNOWLEDGEMENTS. This investigation was supported by the Office of Energy Research, Office of Basic Energy Sciences, Materials Sciences Division of the U.S. Department of Energy (A.P.) and grants from U.S. NSF, Earth Sciences Division (J.F.S.). P.J.G. and M.A.E. acknowledge support from the NIH, J.H.B. from the NSF, and U.W. from the Alexander von Humboldt Foundation.